ADVANCED OPTICAL MATERIALS
www.advopticalmat.de

Bifunctional Integration Performed by a Broadband High-Efficiency Spin-Decoupled Metasurface

Ling-Jun Yang, Sheng Sun, Wei E. I. Sha, and Jun Hu*

Achieving broadband multitasked integration on an ultrathin interface is pivotal to increasing data capacity. However, broadband bifunctional metasurfaces exhibiting high-efficiency and crosstalk-free characteristics are rarely seen. Here, three broadband spin-decoupled criteria are developed to design the meta-atoms of high-efficiency bifunctional metasurfaces. Specifically, six dipole-loaded quasi-I-shaped meta-atoms are proposed to satisfy the broadband spin-decoupled criteria in radio band from 8.6 to 17.8 GHz (about 70% bandwidth) with more than 90% efficiency. The metasurface equipped with the proposed meta-atoms can keep dispersionless phase gradients and crosstalk-free characteristics in two orthogonal circular polarizations. This work demonstrates the broadband scheme with spin-decoupled bifunctional metasurface, yielding two independent broadband multimode vortex beams in two completely decoupled helicities. Besides, other possible applications of the proposed meta-atoms are illustrated from the perspective of the half-wave plant (polarization control). Accordingly, the other multitasked-type bifunctional metasurface is fabricated to achieve the broadband integration of two different functionalities: polarization conversion and full-polarization anomalous refraction. The proposed schemes offer broadband, polarization-multiplexing, and multitasked-integration routes for complex electromagnetic wave manipulations within a subwavelength thickness, which can stimulate the development of electromagnetic/optical integration devices with broadband multiplexing techniques.

1. Introduction

Manipulating electromagnetic (EM) fields at will lays the fundamental basis in many optical and wireless applications. However, traditional EM devices based on natural materials are limited by restricted capabilities, large setups, and low efficiency. Metasurface, an ultrathin artificial interface comprised of subwavelength meta-atoms, can potentially overcome these limitations and has attracted much interest over the last decade due to their various wavefront-shaping capabilities.[1–3] As such, plenty of integrated devices have been developed to address the demands of beam control including holograms,[4,5] metalenses,[6,7] polarization converters,[8,9] and reconfigurable intelligent surfaces.[3,10,11] Furthermore, metasurfaces are excellent candidates for integrating diverse functionalities into single devices with deep-subwavelength thickness and outstanding efficiency.[12–14] However, to meet the explosive demands for large channel capacity and multi-function integration, ongoing efforts should be made to pursue additional multiplexing techniques such as polarization(spin) multiplexing, frequency multiplexing (broadband), space multiplexing, and even multitasking, among others.

Pancharatnam–Berry (PB) phase, an additional phase of scattering-wave triggered by the rotated scatterer, was noted by Prof. Pancharatnam in 1956 and then interpreted as a geometric phase by Prof. Berry in 1984.[15] As the geometric phase is orientation-related but resonance-independent of the meta-atoms, the geometric phase metasurface can potentially extend broadband applications, including vortex beams and polarization conversion.[16–19] However, the geometric-phase-only metasurface can only provide intrinsically opposite signs for two spins, leading to a spin-locked and mirrored functionality for the other circularly polarized (CP) light. In the early years, the "merging" concept was developed to design multi-functional geometric metasurfaces that can generate different holographic images[20] or vortex beams[21] depending on the spin(polarization) states of incident light. Unfortunately, the spin-locked limitations in the "merged" geometric metasurfaces still exist. Due to the inefficient work of partial meta-atoms, these "merged" meta-devices typically suffer from the practical constraints of low efficiencies and functionality crosstalk. Recently, the spin-locked limitation of geometric-phase metasurfaces has been released by involving the dimension-dependent Aharonov–Anandan (AA) phase[22,23] or propagation phase (or dynamic phase).[24–26] Based on this strategy, various spin-decoupled multi-functional metasurfaces have been proposed to realize arbitrary spin-to-orbital momentum converters[27–29] or spin-decoupled wavefront shaping.[30–36] These completely different functions in two

L.-J. Yang, S. Sun, J. Hu
School of Electronic Science and Engineering
University of Electronic Science and Technology of China
Chengdu 611731, P. R. China
E-mail: sunsheng@ieee.org
W. E. I. Sha
College of Information Science & Electronic Engineering
Zhejiang University
Hangzhou 310027, P. R. China
The ORCID identification number(s) for the author(s) of this article can be found under https://doi.org/10.1002/adom.202201955.

DOI: 10.1002/adom.202201955

polarization states pave the way for polarization-multiplexing devices. Some research even exhibits broadband spin-decoupled functions for two generated CP beams.[27,32–36] However, the asymmetric AA-phase meta-atom may introduce unequal reflection amplitudes for two circular polarizations, which may hinder the high-efficiency design. These meta-atoms in the abovementioned spin-decoupled metasurfaces still have room to be broader frequency bandwidths and higher efficiency. Additionally, a systematic understanding of how the broadband spin-decoupled metasurface contributes to broadband functions is still lacking. Efforts should be made to explore potential broadband multitasking integration more than polarization multiplexing.

In this work, we develop three criteria to design broadband spin-decoupled meta-atoms, aiming to engineer bifunctional metasurfaces with two distortion-free CP phase profiles and dispersionless phase gradients. In particular, six dipole-loaded quasi-I-shaped meta-atoms are proposed to satisfy the broadband spin-decoupled criteria, which guarantees stable propagation phase gradients between meta-atoms and more than 90% efficiency at microwave frequencies from 8.6 to 17.8 GHz (about 70% bandwidth). Based on the proposed meta-atoms, we realize two broadband bifunctional metadevices: one simultaneously possessing distinct broadband vortex phases for two CP waves, and the other capable of integrating two distinct broadband functionalities of the full-polarization anomalous refraction and high-efficiency polarization control (See **Figure 1**). The proposed metasurfaces represent a simple but highly efficient broadband anisotropic media to manipulate the phase and polarization of a broadband incident wave, providing strategies for fabricating broadband, high-performance, and integrated EM devices.

2. Theoretical Design and Discussion

The spin-decoupled strategy has been elaborated by combining the propagation and geometric phases.[27–29] The quasi-I-shaped meta-atom has been used to fabricate broadband spin-decoupled metasurfaces.[32,34] The main contributions and organization in this section are as follows: 1) In Section 2.1, we elucidate the broadband spin-decoupled criteria for meta-atoms design, that is, Equations (4–6). 2) In Section 2.2, we develop a broadband high-efficiency spin-decoupled meta-atom. 3) Section 2.3 demonstrates a broadband polarization-multiplexing metasurface that can generate broadband multimode orbital angular momentum (OAM) beams in two spin-decoupled helicity. 4) In Section 2.4, we further explore broadband multitasking-type metasurface that can integrate two distinct functionalities of polarization conversion and wavefront manipulation.

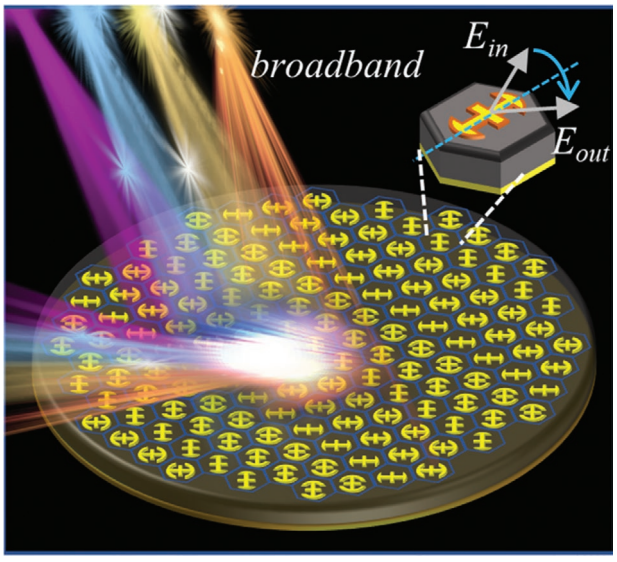

Figure 1. A schematic of a broadband bifunctional metasurface for the full-polarization anomalous refraction and polarization control.

2.1. Three Criteria for Designing Broadband High-Efficiency Spin-Decoupled Meta-Atoms

It is convenient to reveal a spin-decoupled strategy using the Jones calculus.[37] For mirror-symmetric reflection-type meta-atoms, the Jones matrix of CP reflection coefficients can be written as[27]

$$R_{\mathrm{cp}} = \begin{pmatrix} R_{ll}e^{j\phi_{ll}} & R_{lr}e^{j\phi_{lr}} \\ R_{rl}e^{j\phi_{rl}} & R_{rr}e^{j\phi_{rr}} \end{pmatrix} = \begin{pmatrix} \eta e^{-j2\alpha} & \delta \\ \delta & \eta e^{j2\alpha} \end{pmatrix} \tag{1}$$

where δ and η can be calculated as $\delta = (R_{xx}e^{j\phi xx} + R_{yy}e^{j\phi yy})/2$ and $\eta = (R_{xx}e^{j\phi xx} - R_{yy}e^{j\phi yy})/2$. The α is the orientation angle of meta-atoms. Without loss, the reflected amplitudes for x- and y-polarized waves are kept at unity ($R_{xx} = R_{yy} = 1$). If one can obtain a π phase difference between x- and y-polarized reflection phase ($\phi_{xx} - \phi_{yy} = \pi$), δ can be effectively suppressed to zero($\delta = 0$) whilst the converted part η can be reduced to $\eta = e^{j\phi xx}$. Therefore, the imparted phase over left circular polarization (LCP) and right circular polarization (RCP) wave satisfy $\phi_{ll} = \phi_{xx} - 2\alpha$ and $\phi_{rr} = \phi_{xx} + 2\alpha$. We can decompose the CP phases into the even phase and the odd phase as follows.

$$\phi_{\mathrm{even}} = (\phi_{ll} + \phi_{rr})/2 = \phi_{xx} \tag{2}$$

$$\phi_{\mathrm{odd}} = (\phi_{rr} - \phi_{ll})/2 = 2\alpha \tag{3}$$

Equations (2) and (3) establish an insightful relation between propagation, geometric, and two CP phases. Specifically, the propagation phase (ϕ_{xx}) and the geometric phase (2α) contribute the symmetrical (even) phase and antisymmetrical (odd) phase, respectively, to two CP phases. The arbitrary CP phases will be obtained if one can design both the propagation (even) phase and the geometric (odd) phase with an arbitrary phase shift (from 0 to 2π).

Here, we propose three criteria for designing broadband spin-decoupled meta-atoms. 1) The attainable even phase and the odd phase of the proposed meta-atoms must cover a 2π range across the whole bandwidth; 2) The phase gradient between meta-atoms for the even phase and the odd phase must be stable over the whole bandwidth. 3) The conversion efficiency η of meta-atoms must be high enough across the whole bandwidth. For the even phase (propagation phase), we

can design N-number of broadband meta-atoms to satisfy the criteria 1) and 2) as follows:

$$\left|N\cdot\Delta\phi_{xx}\right| = 2\pi \tag{4}$$

$$\Delta\phi_{xx} \approx \phi_{xx}^{i}(f) - \phi_{xx}^{i+1}(f)\,(i \in [1,2,\cdots,N-1]) \tag{5}$$

where the superscript i represents the ith meta-atom. f is the frequency in operating bandwidth. Equations (4) and (5) establish the broadband criteria for the phase coverage and the consistent phase gradient between meta-atoms. For the geometric phase (odd phase), the coverage of 2π can be achieved by altering the orientation angle; the phase and the phase gradient are frequency-independent, making them naturally appropriate for the broadband phase control. It is noticed that the geometric phase can only impart on the co-polarization reflective coefficients (the matrix diagonal elements η) in Equation (1). Therefore, a high-efficiency condition 3) of those geometric-phase meta-atoms should be satisfied within the bandwidth as

$$\left|\eta^{i}(f)\right| = \left|e^{j\phi_{xx}^{i}(f)} - e^{j\phi_{yy}^{i}(f)}\right|/2 \approx 1 (i \in [1,2,\cdots,N]) \tag{6}$$

Equation (6) can be interpreted as the broadband geometric-phase condition (the broadband π phase difference $\phi_{xx}(f) - \phi_{yy}(f) \approx \pi$).[17] It is noticed that $|\eta|^2 + |\delta|^2 = 1$ according to the energy conservation law (without loss). Therefore, a higher η can enhance the efficiency and suppress the crosstalk in cross-polarization. The polarization conversion ratio (PCR = $|\eta|^2/(|\eta|^2 + |\delta|^2) = /\eta|^2$) is commonly used to describe the conversion efficiency.

In all, Equations (4–6) are three specific formulas for designing broadband reflection-type spin-decoupled meta-atoms. The designed metasurface consisting of those broadband meta-atoms can provide a broadband dispersionless phase gradient for two spins(CP) in operating bandwidth as follows:

$$\frac{d\nabla\Phi}{df} = 0 \tag{7}$$

Φ is the phase profile of metasurface for the considered CP. According to the generalized Snell's reflection law,[1] the reflection and diffraction are governed by the phase gradient $\nabla\Phi$ along the interface (the xoy plane).

$$\begin{cases} \nabla\Phi = k_x\hat{e}_x + k_y\hat{e}_y \\ k_0\sin(\theta_r)\cos(\varphi_r) - k_0\sin(\theta_i)\cos(\varphi_i) = k_x \\ k_0\sin(\theta_r)\sin(\varphi_r) - k_0\sin(\theta_i)\sin(\varphi_i) = k_y \end{cases} \tag{8}$$

where θ_i, and φ_i represent the incident polar and azimuth angle, θ_r, and φ_r represent the reflection ones, k_0 is the wave vector in free space, $\hat{e}_x$ and $\hat{e}_y$ are the unit polarization vector, and k_x and k_y can be interpreted as an additional momentum contribution induced by the phase gradient. It is worth mentioning that the proposed broadband spin-decoupled strategy can obtain a frequency-independent (dispersionless) phase gradient in Equation (8) for two spins. Since the phase gradient is essential to shape the wavefront, the proposed broadband strategy may enable us to expand those spin-decoupled functionalities into broadband and high-efficiency cases.

2.2. The Specific Design Process of Broadband High-Efficiency Meta-Atoms

To validate the analytical solutions, we design $N = 6$ number of single-layer dipole-loaded quasi-I-shaped meta-atoms in the microwave region to satisfy the broadband High-efficiency criteria (Equations (4–6)). **Figure 2**a shows the specific arrangement of meta-atoms (left) and corresponding simulation setups of the supercell (right). It is noticed that the triangular arrangement of hexagonal meta-atoms is applied, which can benefit from its compact structure and isotropy in geometric-phase metasurfaces.[19,38] This paper implements a single-layer dielectric substrate to keep simple and ultra-thin characteristics. Periodic boundary conditions are imposed on edge planes of the supercell along x and y directions, and the corresponding reflection coefficient could be obtained from the Floquet port. All the simulation results in this paper are obtained in the commercial software HFSS (High Frequency Structural Simulator). Figure 2b shows the top and side views of the proposed meta-atom. The middle isolation layer is a commercial dielectric board (F4B, $\varepsilon_r = 2.65$, $\sigma = 0.001$) with a thickness of 3 mm. The metal ground plane is printed on the bottom layer to block the transmission wave completely for a high-efficiency reflection. On the top layer, we proposed a dipole-loaded quasi-I-shaped pattern, which consists of a quasi-I-shaped pattern and a dipole, as seen in Figure 2c. The quasi-I-shaped pattern has been utilized in several broadband spin-decoupled metasurfaces.[32,34,39,40] Here the additionally loaded dipole could involve a tunable resonance for Y-pol fields, which is useful for further expanding bandwidth and improving performance.

By optimizing the design parameters of meta-atoms with $d_1 = 7.4$ mm, $d_2 = 3.9$ mm, $d_2 = 1$ mm, $h = 3$ mm, $p = 10$ mm, and $w = 1.2$ mm, we can ensure those proposed meta-atoms to realize a broadband robust geometric phase. In this case, as seen in Figure 2d, the broadband phase shift of the even phase can be obtained by varying the structure parameter R. Simultaneously, the conversion part η maintains almost 0.8 across the frequency from 8.5 to 20 GHz, nearly 80% relative bandwidth. The physical mechanism has been interpreted as the Coriolis effect,[41] where the phase shift of the spin states depends on the varying radians of the ring-shaped structure.[23] The ring-shaped structure has also been applied in the quasi-I-shaped meta-atom to fabricate broadband spin-decoupled metasurfaces.[32,34,39,40] In the proposed meta-atom, the structure parameter R can change the length and radian of the ring-shaped structure, leading to the synchronized phase shift of two CP phases, that is, the phase shift of even phase. A circuit-based interpretation for this result is that the change of the ring-shaped structure by R can synchronously increase (or decrease) the coupling capacitances (or self-inductances) in both x- and y-polarization, leading to a R-related phase shift of the even phase ϕ_{even} (or propagation phase ϕ_{xx}) and keeping the π phase difference between x- and y-polarization ($\phi_{xx} - \phi_{yy} = \pi$). A 180° phase coverage of the even phase is achieved in Figure 2d. Furthermore, by applying a 90° self-rotational operation on

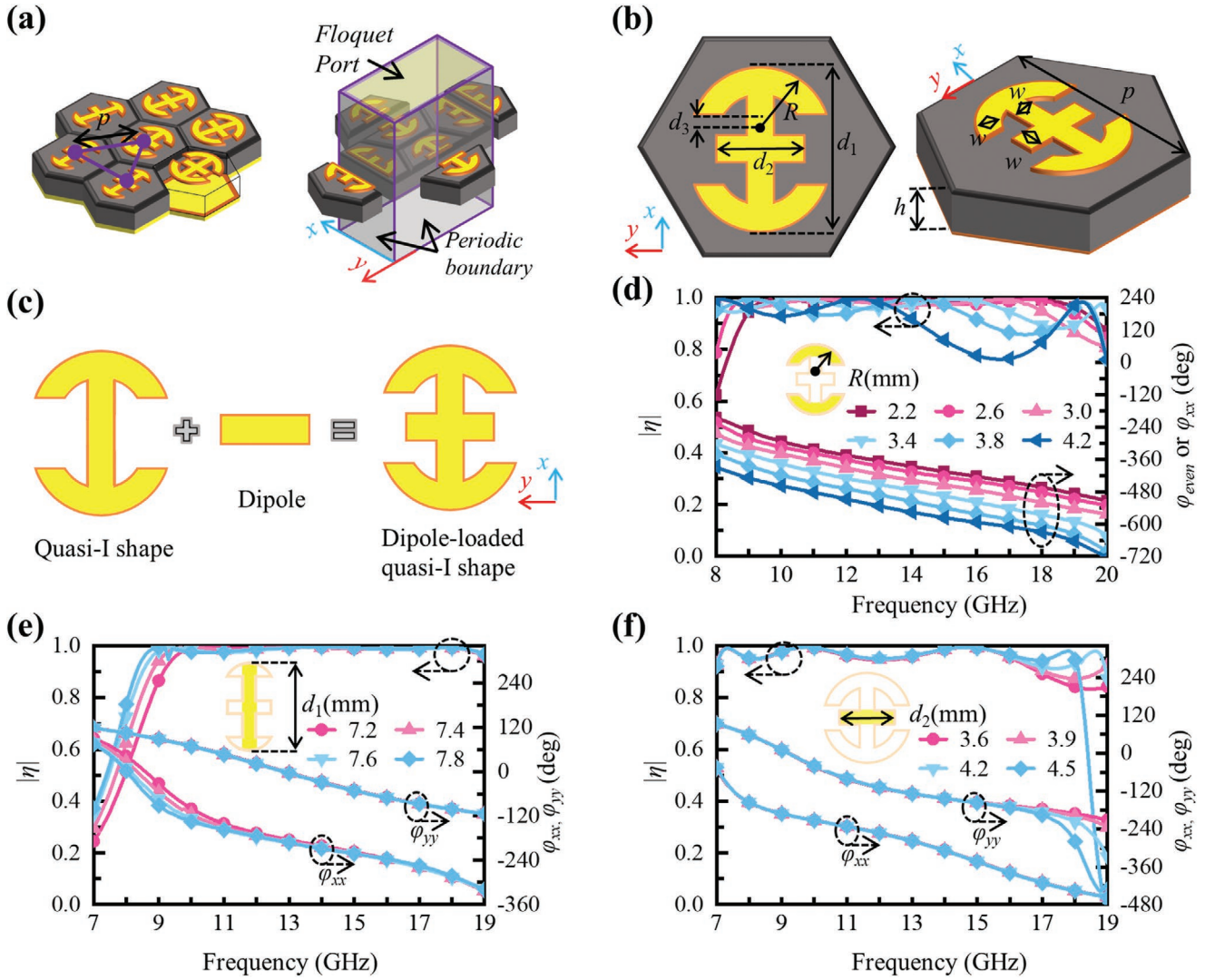

Figure 2. a) Arrangement topology and the simulated cell of meta-atoms. b) are the top and side views of the proposed meta-atom structure. c) is the schematic view of the dipole-loaded quasi-I-shaped pattern. Simulated reflection amplitude and phase responses of meta-atoms with different dimensions d) R, e) d_1, and f) d_2.

these broadband meta-atoms, a full phase span of 360° can be achieved. Hitherto, we can design broadband (80%) spin-decoupled meta-atoms with arbitrary even phases ($N = \infty$) as seen in **Table 1**.

Table 1. Comparisons between the proposed work and several references.

Reference	Operating bandwidth [GHz] (relative bandwidth)	$\|\eta\|$	PCR [%]	N
[34]	16–24 (40%)	0.90	81	4
[27]	15–18 (18.2%)	0.93	86	8
[32]	10–22 (75%)	0.80	64	∞
[33]	7.5–18.5 (80%)	0.90	81	2
This work I	8.5–20 (80%)	0.80	64	∞
This work II	8.6–17.8 (70%)	0.95	90	6

To further improve the conversion efficiency part η in this paper, both parameters d_1 and d_2 are involved in adjusting the π phase difference ($\phi_{xx} - \phi_{yy} \approx \pi$) in the working bandwidth. It is worth mentioning that the parameters d_1 and d_2 of the proposed meta-atom can manipulate the phase responses of ϕ_{xx} and ϕ_{yy} independently as seen in Figure 2e,f. As d_1 varies from 7.2 to 7.8 mm with R and d_2 fixed as 2.2 and 3.9 mm, the low-frequency bandwidth and efficiency part (η) can be designed by independently manipulating the phase ϕ_{xx}. As d_2 varies from 3.6 to 4.5 mm with R and d_1 fixed as 3.6 and 7.3 mm, the high-frequency bandwidth of the efficiency part (η) can be adjusted by independently manipulating the phase ϕ_{yy}. To simplify the design, we use $N = 6$ number of meta-atoms with different parameters R, d_1, and d_2 to discretize the even phase and satisfy the criteria, that is, Equations (4–6). The higher the quantized number N, the higher the beam performance. A 2-bit ($N = 4$) quantized metasurface has been verified to obtain a rather small gain loss and a quite close aperture efficiency

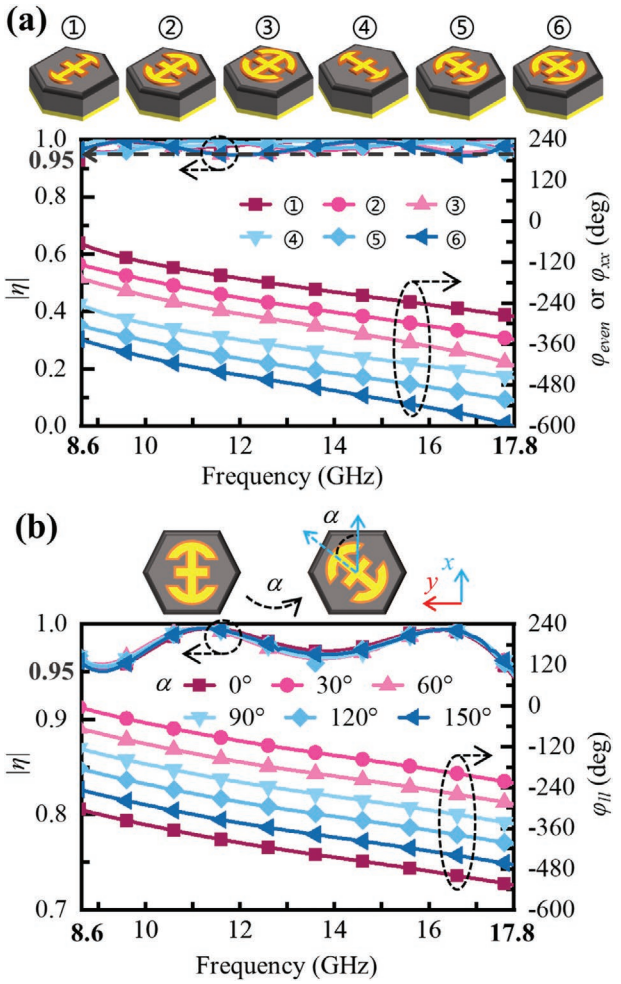

Figure 3. a) Schematic and simulated reflection coefficients of the proposed six non-rotated meta-atoms. b) Reflection coefficients of rotated meta-atoms with different angles α.

compared with the continuous one.[42,43] The specific parameters of meta-atoms i = [1, 2, 3] are R (mm) = [2.2, 3.1, 3.6], d_1 (mm) = [7.7, 7.4, 7.3], and d_2 (mm) = [3.9, 3.9, 4.5]. The parameters of meta-atoms i = [4, 5, 6] are the same with meta-atoms i = [1, 2, 3] except for a 90° self-rotational angle. **Figure 3** shows the schematic and corresponding reflection coefficient of the six proposed meta-atoms. As can be seen from Figure 3a, a near consistent phase difference ($\Delta\phi_{xx}$ = 60°) and a 2π phase coverage of these even phases(ϕ^i_{even} or ϕ^i_{xx}) are always satisfied from 8.6 to 17.8 GHz (70%), and at the same time, the conversion part of these meta-atoms keeps exceeding 0.95 ($|\eta^i| > 0.95$). Figure 3b shows the reflection coefficient of i = 5 meta-atom at different orientation angles to demonstrate the geometric-phase character. By changing the orientation angle α, a strict 2α phase is imparted to the initial meta-atom across the entire bandwidth, which verifies the α-dependent geometric-phase character. Moreover, The amplitudes are almost unchanged and higher than 0.95 for different orientation angles, which is important to engineer a high-efficiency high-performance metasurface without amplitude modulation.[19] In Table 1, we compare our performance with some recently reported studies of spin-decoupled meta-atoms, where the proposed dipole-loaded quasi-I-shaped meta-atoms in this work can significantly enlarge the PCR while maintaining a considerable bandwidth. The PCR of work II can be calculated as PCR = $|\eta|^2 > 90\%$, which means more than 90% of energy can be efficiently converted, and only less than 10% of energy remains as crosstalk. Notice that the crosstalk is uncontrollable and survives in cross-polarization. Therefore, a high PCR is essential to fabricate high-efficiency and low-crosstalk devices, especially for our spin-decoupled (dual-polarization) applications. In all, the high-efficiency and broadband characteristics of proposed meta-atoms can attribute to three aspects:

1) A lower dielectric constant and suitable parameters of period p and thickness h is necessary to achieve a flat phase response (weak-resonant supercells). Triangular arrangement is implemented to weak the coupling between each adjacent meta-atom, achieving ignorable fluctuation of reflection amplitude when the meta-atom rotates ($\Delta|\eta|$ = <0.02 as seen in Figure 3b).
2) The ring-shaped structure (parameter R) is the key point to design the broadband of even phase gradient between meta-atoms and keep a near π phase difference ($\phi_{xx} - \phi_{yy} \approx \pi$) for high efficiency($|\eta^i|$).
3) The phase responses ϕ_{xx} and ϕ_{yy} of the proposed meta-atom can be independently adjusted by the parameters d_1 and d_2, respectively. If the meta-atoms are designed with independent phase responses ϕ_{xx} and ϕ_{yy}, we may design the structural parameters all at once, avoiding the burden triggered by polarization crosstalk. As a result, the complexity of the high-efficiency broadband design procedure will be significantly decreased.

2.3. Broadband Arbitrary OAM Beams over Orthogonal Circular Polarization

Spin-to-orbital devices have been proposed to independently generate single-mode vortex beam in different CP wavefronts.[29] Here, we elaborate how the dispersionless phase gradient contributes to the broadband OAM generation, and then, engineer a broadband OAM metasurface that can generate arbitrary multimode OAM beams over orthogonal circular polarization. Equipped with the proposed broadband meta-atoms, the phase gradient of the fabricated metasurfaces can be kept dispersionless or frequency-independent. The frequency-independent phase gradient for OAM beams can be written as follows:

$$\nabla\Phi(f,\rho',\varphi') = \frac{l}{\rho'}\hat{e}_\varphi \tag{9}$$

where $\rho'$and $\varphi'$are the source point in cylindrical coordinate. l is the topological charge, $\hat{e}_\varphi$ is the unit polarization vector. The phase profile Φ is solved by integrating $\nabla\Phi$ over an arbitrary path.

$$\Phi(f,\rho',\varphi') = \Phi_g(\rho',\varphi') + \Phi_0(f) \tag{10}$$

The first term $\Phi_g(\rho',\varphi')$ is a frequency-independent spiral phase, which is the key point for beam control. The second term $\Phi_0(f)$ is a space-independent but dispersive phase delay for generated beams. In this case, the specific expressions are as follows:

$$\begin{cases}\Phi_g(\rho',\varphi')=l\varphi' \\ \Phi_0(f)=\phi_{xx}(f)+\phi_0\end{cases} \tag{11}$$

where ϕ_0 is a designable phase constant for the phase delay, and in this paper we set $\phi_0=-\phi_{xx}(f=13\ \text{GHz})$. The space-independent phase delay $\Phi_0(f)$ in Equation (11) will not change the wavefront of incident waves, while the frequency-independent spiral phase term Φ_g can efficiently convert a plane wave into the desired OAM beam with the topological charge l in the whole operating bandwidth. The above broadband theoretical process can also expand to generate arbitrary multimode OAM beams. To verify the feasibility of spin-multiplexing meta-atoms and the theoretical broadband model for OAM beams, we engineer a single-layer broadband spin-multiplexing metasurface that can independently control different CP wavefronts into arbitrarily expected multimode OAM beams within a wide bandwidth ranging from 9 to 17 GHz. Arbitrary vortex beam could be generated by involving a phase profile on metasurface as follow.[45]

$$\Phi_g(\varphi_i')=\angle\left(\sum_m a_m e^{jl_m\varphi_i'}\right) \tag{12}$$

where m is the number of OAM modes, l_m and a_m are the OAM modes and the corresponding mode weight, respectively. One can calculate different phase profiles Φ_L and Φ_R for different LCP and RCP by Equation (12). For example, we try to generate a single-mode OAM beam with parameter $l_L=[5]$, $a_L=[1]$ for LCP and a multimode OAM beam with parameter $l_R=[-2,6]$, $a_R=[0.38,0.62]$ for RCP. **Figure 4**a shows the specific phase profiles Φ_L, Φ_R, Φ_{even}, and Φ_{odd}, calculated by Equations (2), (3), and (12). Then the specific configuration of the metasurface can be designed by the following process as seen in Figure 4b: First, arranging these proposed meta-atoms according to the even phase profile Φ_{even}, that is, the propagation phase of meta-atoms satisfy $\Phi_{xx}=\Phi_{even}$. Second, rotating the orientation angle of meta-atoms satisfy $\alpha=\Phi_{odd}/2$.

Figure 5 shows the broadband performance of the simulating normalized co-polarization far-field patterns under the normal incidence of the LCP or RCP plane wave. In this paper, three frequency points of 9, 13, and 17 GHz are selected to verify our broadband performance, which corresponds to the low, medium, and high frequencies of the operating bandwidth, respectively. The observation range of far-field patterns $E(\theta, \varphi)$ is the upper-space, meaning the polar angle $\theta=[0{:}1{:}90]$ and azimuth angle $\varphi=[0{:}1{:}360]$ (degree). The corresponding OAM spectra are also included to analyze the OAM purity based on the Discrete Fourier Transform as follow:

$$A_l(\theta,l)=\sum_{\varphi=1}^{360}E(\theta,\varphi)e^{-jl\varphi*2\pi/360} \tag{13}$$

Under the normal incidence of the LCP plane wave, the co-polarization scattering fields show the strictly five-period helical phase at the main lobe; the corresponding normalized OAM spectra also demonstrate the high-purity generation of $l_L=[5]$ OAM beams. By switching the incidence wave from LCP to RCP, the metasurface can also achieve the high-purity generation of multimode OAM beams with $l_R=[-2,6]$. The clear phase shift in phase patterns and the high purity of OAM modes in spectra at 9, 13, and 17 GHz in Figure 5 verify the broadband performance of this proposed metasurface. The polarization conversion ratio of metasurface is also included in Figure 5 to verify the conversion efficiency and calculated as

$$\text{PCR}_{\text{metasurface}}=\frac{\iint_s\left|E_{\text{co-pol}}\right|^2 ds}{\iint_s\left|E_{\text{co-pol}}\right|^2 ds+\iint_s\left|E_{\text{cross-pol}}\right|^2 ds} \tag{14}$$

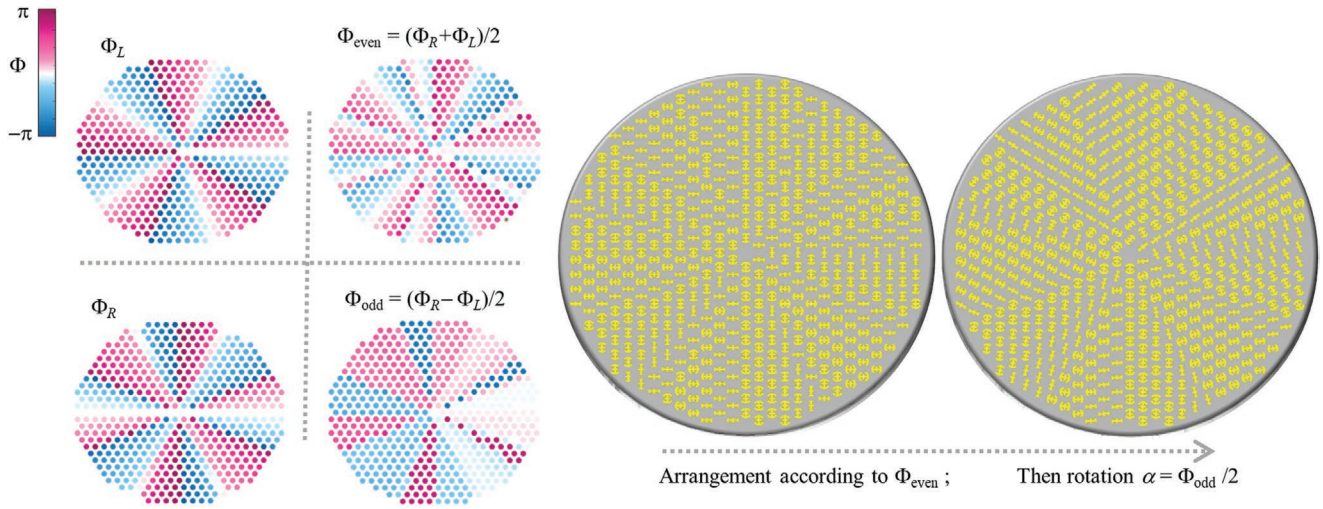

Figure 4. Design process of the broadband spin-decoupled metasurface for generating a single-mode OAM beam with parameter $l_L=[5]$, $a_L=[1]$ for LCP and a multimode OAM beam with parameter $l_R=[-2,6]$, $a_R=[0.38,0.62]$ for RCP. a) Specific phase profiles Φ_L, Φ_R, Φ_{even}, and Φ_{odd}, b) specific configuration of metasurface.

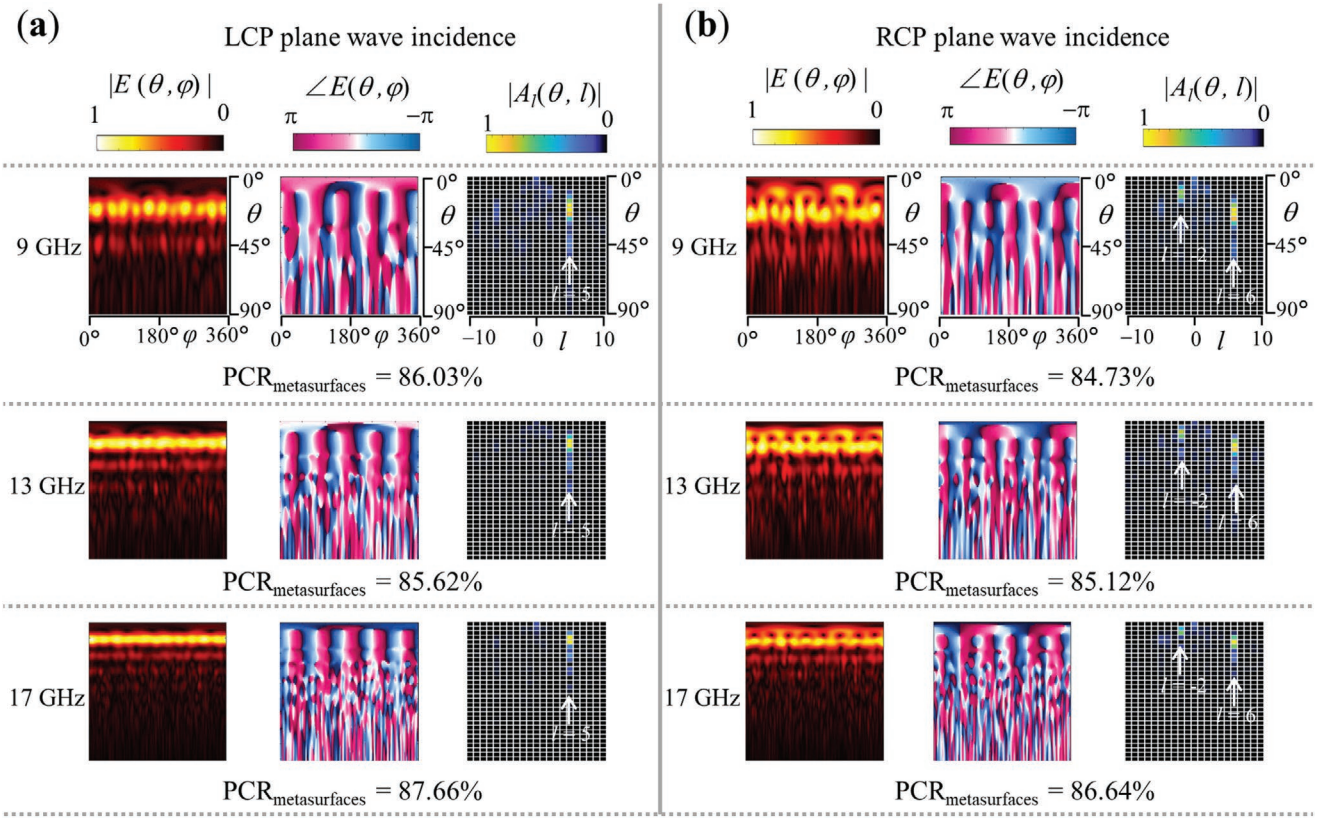

Figure 5. Far-field amplitude pattern, phase pattern, and corresponding spectral analyses of co-polarization scattering *E*-field at 9, 13, and 17 GHz for the broadband spin-decoupled metasurface under the normal incidence of a) the LCP plane wave, b) the RCP plane wave; the polarization conversion ratio of metasurfaces are also included.

where $E_{\text{co-pol}}$ and $E_{\text{cross-pol}}$ are the co-polarization and the cross-polarization scattering *E*-field, respectively. *S* is the mentioned observation range on upper space. It is noticed that the polarization conversion ratio of metasurface possesses a high level of more than 84% at the observing frequencies in both LCP and RCP cases. This is significant for high-efficiency dual-polarization applications.

2.4. Broadband Bifunctional Integration of Polarization Control and Full-Polarization Wavefront Shaping

The linearly polarized (LP) Jones matrix of the proposed six meta-atoms can be approximately rewritten into the half-wave-plate term yet with a controllable even phase (ϕ_{even} or ϕ_{xx}) for both orthogonal LP waves as seen in **Figure 6**. Therefore, beyond the spin-decoupled bifunctional integration, these meta-atoms can be naturally extended to broadband half-wave-plate-related devices,[46,47] simultaneously imparting with a broadband full-polarization phase gradient. Specifically, the half-wave-plate meta-atoms can flip the polarization vector of the incident wave along the principal axis, supporting broadband polarization control.[48–50] The controllable full-polarization phase gradient opens a new degree of freedom to integrate additional wavefront-shaping functions including cloak,[40] vortex beam,[51,52] image,[53,54] and anomalous reflection.[55,56] Here, we demonstrate a multi-functional metasurface that integrates two broadband functions of polarization conversion and full-polarization anomalous reflection. By rotating 45° of the proposed meta-atoms, the 45°-rotated Jones matrix of LP reflection coefficients can be written as[27]

$$R_{\text{LP}}^{(\alpha=45^\circ)} = M^{(\alpha=45^\circ)} R_{\text{LP}} M^{-1(\alpha=45^\circ)} = \begin{pmatrix} \delta & \eta \\ \eta & \delta \end{pmatrix} \tag{15}$$

where M ($\alpha = 45°$) is the rotation matrix with rotation angle $\alpha = 45°$. Therefore, the 45°-rotated meta-atoms can work as a broadband polarization converter in which the reflection coefficients satisfy $|R_{ll}| = |R_{rr}| = |R_{xy}| = |R_{yx}| = |\eta|$. Here, the mentioned polarization conversion is compared to the result obtained by traditional metal ground (GND), as seen in Figure 6b. Additionally, an anomalous reflection can be imparted into this polarization converter, and one can calculate the anomalous reflection angle θ_r according to the phase gradient in Equation (8). In this scheme, we design a phase gradient to obtain a deviation angle of beams $\theta_r = 20°$ apart from the *z*-axis with $\varphi_r = 0°$ for a normal incident plane wave at 13 GHz. We engineered a metasurface consisting of 45°-rotated meta-atoms with the obtained phase gradient to introduce the anomalous reflection at the interface. The 3D full-wave simulation is performed in the numerical simulation software HFSS. **Figure 7** shows the simulated normalized far-field patterns on the *xoz*-plane under the normal plane-wave incidence of four representative polarizations (LCP, RCP, X-LP, and Y-LP) at 9, 13, and 17 GHz, respectively. The

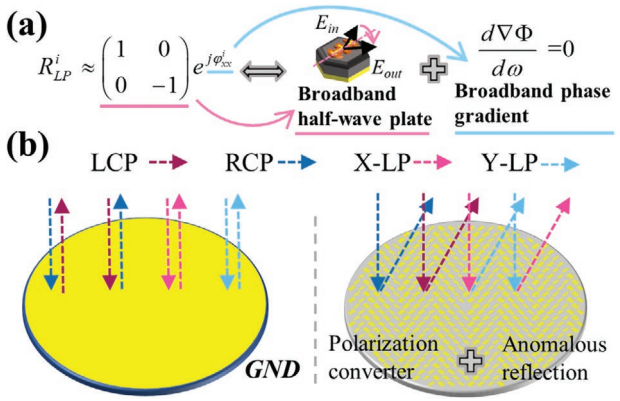

Figure 6. a) The LP Jones matrix of proposed six meta-atoms and corresponding functions. b) Traditional reflection on metal ground (GND) and the anomalous reflection on the proposed polarization–conversion metasurface.

converted far-field results are significantly higher (10 dB) than the unconverted one. Additionally, all the converted fields are bended into the desired direction and match quite well with the theoretical predictions given by Equation (8). These suggest that two different functions, polarization conversion and full-polarization anomalous reflection, can be simultaneously integrated into a single-layer metasurface to realize aperture-shared devices. Moreover, the multi-function metasurface equipped with proposed broadband meta-atoms can perform well across the operating bandwidth from 9 to 17 GHz.

3. Conclusion

In this work, a scheme for the broadband high-efficiency bifunctional integration by single-layer metasurface has been proposed, implemented, and experimentally verified. First, three criteria have been proposed to design broadband spin-decoupled meta-atoms. Accordingly, we have proposed six dipole-loaded quasi-I-shaped meta-atoms with a considerable bandwidth (about 70%) and a higher efficiency (PCR >90%) compared with existing meta-atoms. This high-efficiency character is essential for low-crosstalk multifunctional devices. Then, a broadband spin-decoupled OAM metasurface has been theoretically designed and verified by simulation, indicating that the metasurface using the proposed meta-atoms can maintain two different phase gradients for two CP in operating bandwidth. The findings can be used to engineer broadband polarization-multiplexing devices. In addition, based on the proposed meta-atoms, the other multitasked-type bifunctional metasurface is fabricated to achieve the broadband integration of full-polarization anomalous reflection and high-efficiency polarization conversion. This polarization-related example contributes to existing knowledge of spin-decoupled meta-atoms by providing another multitasked-integration route of broadband polarization control and full-polarization wavefront shaping.

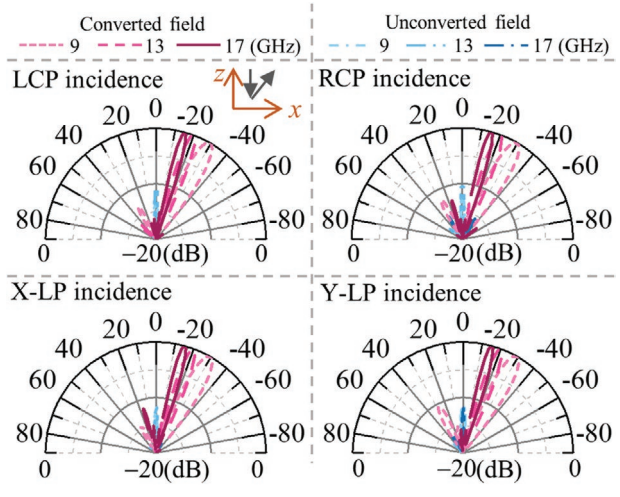

Figure 7. Normalized far-field simulated patterns on the *xoz*-plane under the normal plane-wave incidence of four representative polarizations at 9, 13, and 17 GHz. Here, the converted and unconverted fields are the comparison results of polarization with the traditional metal ground (GND).

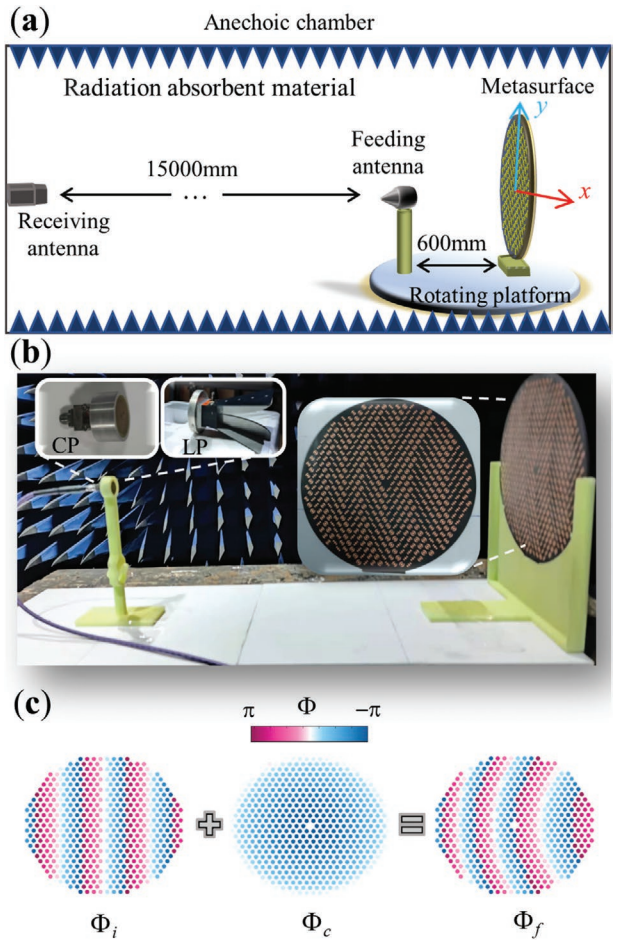

Figure 8. a) Experimental setup of far-field measurement in the microwave anechoic chambers. b) The photograph of the specific devices on the rotating platform, including the feeding antennas and the fabricated bifunctional metasurface. c) The initial, compensated, and final phase profiles of metasurface in the design process corresponding to the Φ_i, Φ_c, and Φ_f.

4. Experimental Section

To further verify the proposed method, an experiment is implemented as shown in **Figure 8**. Figure 8a shows the experimental setup in a microwave anechoic chamber. The receiving antenna was about 15 m away from the rotating platform to detect the converted and unconverted far-field patterns. Figure 8b shows the photograph of the specific devices on the platform, including the feeding antenna and the fabricated bifunctional metasurface. Two broadband CP Archimedes spiral antennas and a broadband LP horn antenna with the bandwidth from 8 to 17 GHz were separately placed in the front of the metasurface at a distance of 600 mm and work as feeding antennas to impinge four representative beams (LCP, RCP, X-LP, and Y-LP). An additional compensated phase was imparted into this fabricated metasurface to compensate for the spherical wave generated by the feeding antenna. The compensated phase Φ_c for the meta-atom satisfies the method described in ref. [17] at 13 GHz. The final phase profile Φ_f can be obtained by the superposition of Φ_i (initial phase profile for anomalous reflection) and Φ_c as seen in Figure 8c. According to this phase profile, the metasurface can be fabricated by the proposed meta-atoms using the printed circuit board technique, and the metallic layer is copper with a thickness of 0.035 mm. **Figure 9** shows the experimentally normalized far-field patterns in the *xoz*-plane obtained by rotating the platform. Figure 9a shows both converted field and unconverted results by impinging LCP, RCP, X-LP, and Y-LP beams, respectively. Within the operating bandwidth of the feeding antenna 8–17 GHz, the obvious beam bending effect occurs in converted fields with significant suppression in unconverted fields, which verified the bifunctional integration of broadband full-polarization

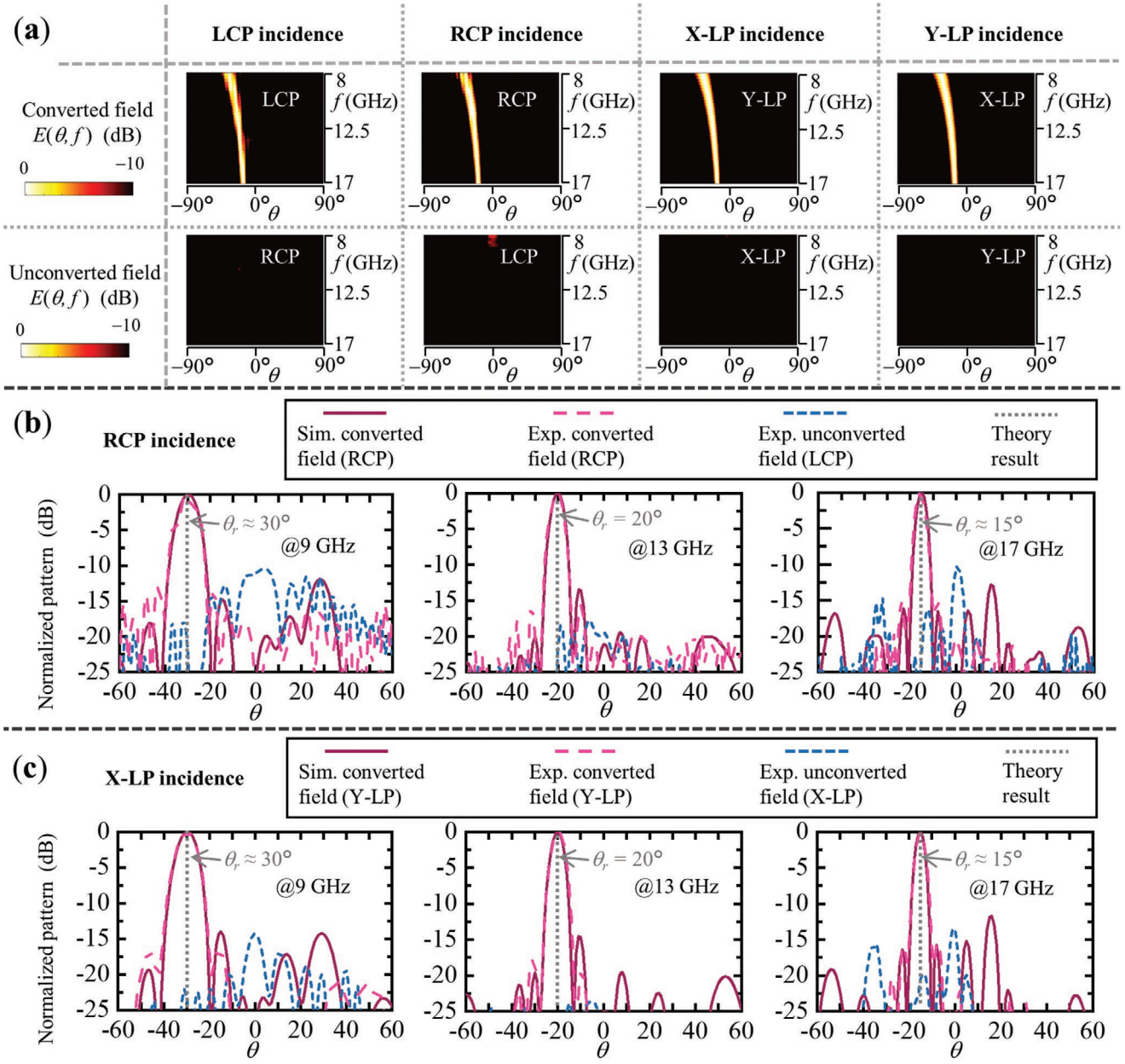

Figure 9. The normalized far-field patterns of converted and unconverted polarization in the *xoz*-plane. a) the broadband results under the incidence of the four representative beams (LCP, RCP, X-LP, and Y-LP) from 8 to 17 GHz. b,c) shows the specific patterns under the incidence of RCP and X-LP beams at 9, 13, and 17 GHz, where the theoretically calculated and the simulated results are also included.

anomalous reflection and high-efficiency polarization conversion. Figure 9b,c shows the specific patterns under the incidence of RCP and X-LP beams at 9, 13, and 17 GHz, where the theoretically calculated and simulated far-field results are also included. As is shown, all results agree well, illustrating a noticeable beam bending effect with reflection angle θ_r about 30°, 20°, and 15° at 9, 13, and 17 GHz. Simultaneously, benefitting from the phase-compensated design, the main lobes of experimental results impinged by the spherical wave were consistent with the simulated ones impinged by the plane wave. The reflection fields were effectively converted into the expected polarization with small enough (more than −10 dB) crosstalk (unconverted polarization). These experiment results verified the high-efficiency broadband multifunctions scheme that achieves the broadband integration of high-efficiency polarization control and full-polarization wavefront shaping.

Acknowledgements

This work was supported in part by the National Natural Science Foundation of China under Grant 61971115, Grant 61721001, Grant 61975177.

Conflict of Interest

The authors declare no conflict of interest.

Data Availability Statement

The data that support the findings of this study are available from the corresponding author upon reasonable request.

Keywords

bifunctional metasurface, broadband metasurface, orbital angular momentum, Pancharatnam–Berry phase, polarization conversion

Received: August 22, 2022
Revised: October 20, 2022
Published online: November 17, 2022

[1] N. Yu, P. Genevet, M. A. Kats, F. Aieta, J.-P. Tetienne, F. Capasso, Z. Gaburro, *Science* **2011**, *334*, 333.
[2] S. Sun, Q. He, S. Xiao, Q. Xu, X. Li, L. Zhou, *Nat. Mater.* **2012**, *11*, 426.
[3] X. G. Zhang, W. X. Jiang, H. L. Jiang, Q. Wang, H. W. Tian, L. Bai, Z. J. Luo, S. Sun, Y. Luo, C.-W. Qiu, T. J. Cui, *Nat. Electron.* **2020**, *3*, 165.
[4] J. P. B. Mueller, N. A. Rubin, R. C. Devlin, B. Groever, F. Capasso, *Phys. Rev. Lett.* **2017**, *118*, 113901.
[5] Y. Yuan, K. Zhang, B. Ratni, Q. Song, X. Ding, Q. Wu, S. N. Burokur, P. Genevet, *Nat. Commun.* **2020**, *11*, 4186.
[6] R. Jin, L. Tang, J. Li, J. Wang, Q. Wang, Y. Liu, Z.-G. Dong, *ACS Photonics* **2020**, *7*, 512.
[7] K. Zhang, Y. Yuan, D. Zhang, X. Ding, B. Ratni, S. N. Burokur, M. Lu, K. Tang, Q. Wu, *Opt. Express* **2018**, *26*, 1351.
[8] B. Kamal, J. Chen, Y. Yingzeng, J. Ren, S. Ullah, W. U. R. Khan, *Opt. Mater. Express* **2021**, *11*, 1343.
[9] W.-L. Guo, G.-M. Wang, K. Chen, H.-P. Li, Y.-Q. Zhuang, H.-X. Xu, Y. Feng, *Phys. Rev. Appl.* **2019**, *12*, 014009.
[10] X. Bai, F. Kong, Y. Sun, G. Wang, J. Qian, X. Li, A. Cao, C. He, X. Liang, R. Jin, W. Zhu, *Adv. Opt. Mater.* **2020**, *8*, 2000570.
[11] L. Li, T. Jun Cui, W. Ji, S. Liu, J. Ding, X. Wan, Y. Bo Li, M. Jiang, C.-W. Qiu, S. Zhang, *Nat. Commun.* **2017**, *8*, 197.
[12] M. R. Akram, G. Ding, K. Chen, Y. Feng, W. Zhu, *Adv. Mater.* **2020**, *32*, 1907308.
[13] D. Wang, K. Liu, X. Li, G. Wang, S. Tang, T. Cai, *Nanophotonics* **2022**, *11*, 1177.
[14] H.-X. Xu, C. Wang, G. Hu, Y. Wang, S. Tang, Y. Huang, X. Ling, W. Huang, C.-W. Qiu, *Adv. Opt. Mater.* **2021**, *9*, 2100190.
[15] M. V. Berry, *Proc. R. Soc. Lond., Math. Phys. Sci.* **1984**, *392*, 45.
[16] H.-X. Xu, H. Liu, X. Ling, Y. Sun, F. Yuan, *IEEE Trans. Antennas Propag.* **2017**, *65*, 7378.
[17] L.-J. Yang, S. Sun, W. E. I. Sha, *IEEE Trans. Antennas Propag.* **2020**, *68*, 2166.
[18] Y. Ran, J. Liang, T. Cai, H. Li, *Opt. Commun.* **2018**, *427*, 101.
[19] L. Yang, S. Sun, W. E. I. Sha, *Adv. Opt. Mater.* **2021**, *9*, 2001711.
[20] D. Wen, F. Yue, G. Li, G. Zheng, K. Chan, S. Chen, M. Chen, K. F. Li, P. W. H. Wong, K. W. Cheah, E. Y. B. Pun, S. Zhang, X. Chen, *Nat. Commun.* **2015**, *6*, 8241.
[21] C. Zhang, F. Yue, D. Wen, M. Chen, Z. Zhang, W. Wang, X. Chen, *ACS Photonics* **2017**, *4*, 1906.
[22] R. Ji, X. Xie, X. Guo, Y. Zhao, C. Jin, K. Song, S. Wang, J. Yin, Y. Liu, C. Jiang, C. Yang, X. Zhao, W. Lu, *ACS Photonics* **2021**, *8*, 1847.
[23] G. D. Bai, Q. Ma, R. Q. Li, J. Mu, H. B. Jing, L. Zhang, T. J. Cui, *Phys. Rev. Appl.* **2019**, *12*, 044042.
[24] Y. Qiu, S. Tang, T. Cai, H. Xu, F. Ding, *Front. Guided Wave Opt. Optoelectron.* **2021**, *14*, 134.
[25] S. Li, Z. Wang, S. Dong, S. Yi, F. Guan, Y. Chen, H. Guo, Q. He, L. Zhou, S. Sun, *Nanophotonics* **2020**, *9*, 3473.
[26] Y. Yuan, K. Zhang, X. Ding, B. Ratni, S. N. Burokur, Q. Wu, *Photonics Res.* **2019**, *7*, 80.
[27] G. Ding, K. Chen, X. Luo, J. Zhao, T. Jiang, Y. Feng, *Phys. Rev. Appl.* **2019**, *11*, 044043.
[28] H.-X. Xu, L. Han, Y. Li, Y. Sun, J. Zhao, S. Zhang, C.-W. Qiu, *ACS Photonics* **2019**, *6*, 211.
[29] R. C. Devlin, A. Ambrosio, N. A. Rubin, J. P. B. Mueller, F. Capasso, *Science* **2017**, *358*, 896.
[30] H.-X. Xu, G. Hu, M. Jiang, S. Tang, Y. Wang, C. Wang, Y. Huang, X. Ling, H. Liu, J. Zhou, *Adv. Mater. Technol.* **2020**, *5*, 1900710.
[31] Z. X. Wang, J. W. Wu, L. W. Wu, Y. Gou, H. F. Ma, Q. Cheng, T. J. Cui, *Adv. Opt. Mater.* **2021**, *9*, 2001609.
[32] W.-L. Guo, G.-M. Wang, W.-Y. Ji, Y.-L. Zheng, K. Chen, Y. Feng, *IEEE Trans. Antennas Propag.* **2020**, *68*, 3534.
[33] W.-L. Guo, G.-M. Wang, X.-Y. Luo, H.-S. Hou, K. Chen, Y. Feng, *Ann. Phys.* **2020**, *532*, 1900472.
[34] Y. Gou, H. F. Ma, L. W. Wu, Z. X. Wang, P. Xu, T. J. Cui, *ACS Omega* **2021**, *6*, 30019.
[35] M. Liu, P. Huo, W. Zhu, C. Zhang, S. Zhang, M. Song, S. Zhang, Q. Zhou, L. Chen, H. J. Lezec, A. Agrawal, Y. Lu, T. Xu, *Nat. Commun.* **2021**, *12*, 2230.
[36] Q. Zhang, Q. Zhang, R. Xie, R. Xie, Z. Gu, H. Zhang, C. Chen, C. Chen, J. Ding, J. Ding, W. Chen, *Opt. Express* **2022**, *30*, 4249.
[37] C. Menzel, C. Rockstuhl, F. Lederer, *Phys. Rev. A* **2010**, *82*, 053811.
[38] D. Sievenpiper, L. Zhang, R. F. J. Broas, N. G. Alexopolous, E. Yablonovitch, *IEEE Trans. Microw. Theory Tech.* **1999**, *47*, 2059.
[39] H.-X. Xu, S. Wang, C. Wang, M. Wang, Y. Wang, Q. Peng, *IEEE Trans. Antennas Propag.* **2022**, *70*, 1895.
[40] H.-X. Xu, G. Hu, Y. Wang, C. Wang, M. Wang, S. Wang, Y. Huang, P. Genevet, W. Huang, C.-W. Qiu, *Light: Sci. Appl.* **2021**, *10*, 75.
[41] K. Y. Bliokh, Y. Gorodetski, V. Kleiner, E. Hasman, *Phys. Rev. Lett.* **2008**, *101*, 030404.
[42] D. Zhang, X. Cao, H. Yang, J. Gao, S. Lv, *Chin. Phys. B* **2019**, *28*, 034204.
[43] M. Smith, Y. Guo, *IEEE Trans. Antennas Propag.* **1983**, *31*, 821.

[44] J. Y. Yin, J. Ren, Q. Zhang, H. C. Zhang, Y. Q. Liu, Y. B. Li, X. Wan, T. J. Cui, *IEEE Trans. Antennas Propag.* **2016**, *64*, 5181.
[45] L.-J. Yang, S. Sun, W. E. I. Sha, Z. Huang, J. Hu, *IEEE Trans. Antennas Propag.* **2022**, *70*, 573.
[46] F. Ding, Z. Wang, S. He, V. M. Shalaev, A. V. Kildishev, *ACS Nano* **2015**, *9*, 4111.
[47] A. Pors, M. G. Nielsen, S. I. Bozhevolnyi, *Opt. Lett.* **2013**, *38*, 513.
[48] J. Fan, Y. Cheng, *J. Phys. Appl. Phys.* **2019**, *53*, 025109.
[49] M. Wang, Y. Cheng, L. Wu, *Appl. Opt.* **2022**, *61*, 4833.
[50] Y. Cheng, X. Zhu, J. Li, F. Chen, H. Luo, L. Wu, *Phys. E* **2021**, *134*, 114893.
[51] B. He, J. Liu, Y. Cheng, F. Chen, H. Luo, X. Li, *Phys. E* **2022**, *144*, 115373.
[52] B. He, J. Fan, Y. Cheng, F. Chen, H. Luo, R. Gong, *J Opt. Soc. Am. B* **2021**, *38*, 1518.
[53] Z.-L. Deng, Q.-A. Tu, Y. Wang, Z.-Q. Wang, T. Shi, Z. Feng, X.-C. Qiao, G. P. Wang, S. Xiao, X. Li, *Adv. Mater.* **2021**, *33*, 2103472.
[54] K. Toda, M. Tamamitsu, T. Ideguchi, *Light: Sci. Appl.* **2021**, *10*, 1.
[55] X. Zhu, Y. Cheng, J. Fan, F. Chen, H. Luo, L. Wu, *Diamond Relat. Mater.* **2022**, *121*, 108743.
[56] X. Zhu, Y. Cheng, F. Chen, H. Luo, W. Ling, *J. Opt. Soc. Am. B* **2022**, *39*, 705.